AIP | Physics of Plasmas

Modelling of radiative divertor operation towards detachment in experimental advanced superconducting tokamak

YiPing Chen, F. Q. Wang, X. J. Zha, L. Q. Hu, H. Y. Guo et al.

Citation: Phys. Plasmas **20**, 022311 (2013); doi: 10.1063/1.4791659
View online: http://dx.doi.org/10.1063/1.4791659
View Table of Contents: http://pop.aip.org/resource/1/PHPAEN/v20/i2
Published by the AIP Publishing LLC.

Modelling of radiative divertor operation towards detachment in experimental advanced superconducting tokamak

YiPing Chen,[1,a)] F. Q. Wang,[1] X. J. Zha,[2] L. Q. Hu,[1] H. Y. Guo,[1] Z. W. Wu,[1] X. D. Zhang,[1] B. N. Wan,[1] and J. G. Li[1]
[1]*Institute of Plasma Physics, Chinese Academy of Sciences, Hefei, Anhui 230031, China*
[2]*Department of Applied Physics, College of Sciences, Donghua University, Shanghai 201620, China*

(Received 28 December 2012; accepted 23 January 2013; published online 28 February 2013)

In order to actively control power load on the divertor target plates and study the effect of radiative divertor on plasma parameters in divertor plasmas and heat fluxes to the targets, dedicated experiments with Ar impurity seeding have been performed on experimental advanced superconducting tokamak in typical L-mode discharge with single null divertor configuration, ohmic heating power of 0.5 MW, and lower hybrid wave heating power of 1.0 MW. Ar is puffed into the divertor plasma at the outer target plate near the separatrix strike point with the puffing rate $1.26 \times 10^{20}\ s^{-1}$. The radiative divertor is formed during the Ar puffing. The SOL/divertor plasma in the L-mode discharge with radiative divertor has been modelled by using SOLPS5.2 code package [V. Rozhansky *et al.*, Nucl. Fusion **49**, 025007 (2009)]. The modelling shows the cooling of the divertor plasma due to Ar seeding and is compared with the experimental measurement. The changes of peak electron temperature and heat fluxes at the targets with the shot time from the modelling results are similar to the experimental measurement before and during the Ar impurity seeding, but there is a major difference in time scales when Ar affects the plasma in between experiment and modelling. © *2013 American Institute of Physics*. [http://dx.doi.org/10.1063/1.4791659]

I. INTRODUCTION

Heat and particle controllability in the divertor has become one of the important issues on experimental advanced superconducting tokamak (EAST). The total heating and driving power will be increased on EAST in the next years; the plasma temperature and heat fluxes to the target plates of divertor will increase with the heating power. In order to control the divertor power loads in the long pulse discharge the radiative divertor with partial or full detachment will become an important operation regime in EAST. Experiments to address the issue of radiative divertor have been carried out, and the divertor detachment has been achieved by gas puffing or impurity seeding in the divertor plasmas on EAST.[1] For understanding the processes of detachment and supporting the experimental measurement in divertor plasmas, the modelling study on radiative divertor in EAST is necessary. The modelling study on the radiative divertor in EAST is performed by using SOLPS5.2 code package,[2] one of the latest version of SOLPS(B2-Eirene).[3,4] SOLPS5.2 couples the plasma fluid code B2 (Refs. 3–5) to the neutral Monte-Carlo code Eirene[6,7] and has become an important modelling tool of SOL/divertor plasma in tokamak.

The radiative divertor can be produced by the impurity seeding; the heat fluxes to the targets are reduced in the radiative divertor due to the impurity radiation. The power loss from the impurity radiation is evaluated by $Wr = -n_e n_z Lz(T_e)$, n_e is the electron density, n_z is the impurity density, and $Lz(T_e)$[8,9] is the emission rate coefficient. Concerning the dependency on electron temperature T_e, C and N_2 are ideally suited to radiate in the rather cold scrape-off layer, but C has two problems.[10] First, C tends to form MARFEs which can lead to disruptions. Second, it is difficult to control: it is eroded from target plates and from the walls continuously by physical and chemical sputtering, and it is not exhausted but redeposited. Nitrogen builds up large wall inventories, which may cause problems when steady-state operation is approached. On the other hand, N_2 is well suited for experiments lacking active pumping.[10] The noble gases Ne and Ar radiate at higher temperatures than C and N. As they recycle fully, they can be pumped and thereby be controlled.[10] With the increase of heating power the temperature of divertor plasma will be increased in EAST, so the study of the radiative divertor produced by impurity (Ar) or (Ne) seeding plays an important role in EAST with higher heating power and steady-state operation in the next years. At present, the divertor targets and first wall on EAST are covered by carbon materials, so EAST is a carbon machine. When impurity (Ar) or (Ne) is seeded into the plasma it is likely to be mixed with C in the discharges; the radiation from C and the problems with C mentioned above may exist.

II. MODELLING OF RADIATIVE DIVERTOR OPERATION TOWARDS DETACHMENT

Dedicated experiments on radiative divertor with Ar impurity seeding have been performed on EAST in typical L-mode discharge with single null divertor configuration. The main parameters in the shot include ohmic heating power $P_{ohm} = 0.519$ MW, lower hybrid wave (LH) heating power $P_{LH} = 1.0$ MW, plasma current $I_p = 0.6$ MA, and toroidal field $B_t = 2.0\,T$. The particle balance is maintained by the gas puffing near the inner midplane and pumping. During the shot time $t = 4$–4.4 s the Ar impurity is seeded near the separatrix strike point at the outer target plate in order to study the radiative divertor operation with Ar seeding.

[a)]E-mail: ypchen@ipp.ac.cn.

TABLE I. Main parameters in the typical L-mode discharge with radiative divertor operation on EAST.

Shot time	t [s]	0-5.0
Major radius	R [m]	1.858
Minor radius	a [m]	0.439
Aspect ratio	A	4.232
Plasma current	I_p [MA]	0.599
Loop voltage	V_{loop} [V]	0.865
Toroidal field	B_0 [T]	2.012
Elongation	κ	1.759
Triangularity	δ_u	0.329
Triangularity	δ_l	0.528
Line-averaged density	$\bar{n}_e$ [10^{19} m^{-3}]	2.82
Total heating power	P_t [MW]	1.473
LH heating power	P_{LH} [MW]	0.954
Ohmic heating power	P_{ohm} [MW]	0.519
Configuration	···	Single null

The main shot parameters in the typical L-mode discharge are shown in the Table I. The plasma current I_p, the loop voltage V_{loop}, the line-averaged electron density $\bar{n}_e$, and LH heating power P_{LH} trace versus time in the shot are shown in Fig. 1. The peak electron temperature T_e and density n_e, peak heat flux q_t, and ion saturation flux J_s to the target plates trace versus time in the shot are shown in Fig. 2. The "peak values" here refer to the maximum values measured by the stationary probes during the discharge, and these values do not necessarily represent the peak values of the radial profiles, because the full profiles were not measured.

From Fig. 1, the line-averaged electron density $\bar{n}_e$ and loop voltage V_{loop} increase and plasma current I_p decreases when Ar is seeding, which happens after the shot time $t = 4.4$ s. $\bar{n}_e$, V_{loop}, and I_p begin to respond to Ar seeding at the shot time $t = 4.4$ s which is about 0.4 s later than the starting time of Ar seeding at the shot time $t = 4.0$ s, which means that before Ar arrives at the core plasma it needs about 0.4 s to travel to the core plasma from the seeding tube entrance. The seeding tube entrance is the inlet through which the Ar gas is seeded into the plasma, and it locates outside the torus. From Fig. 2, at the target plates, the peak electron temperature

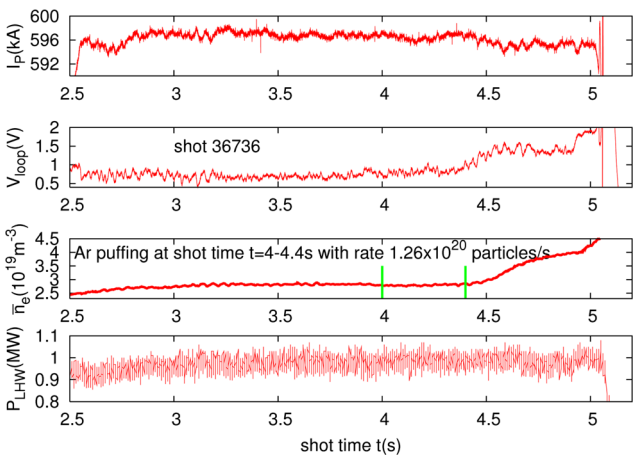

FIG. 1. The plasma current I_p, the loop voltage V_{loop}, the line-averaged electron density $\bar{n}_e$ and LH heating power P_{LH} trace versus shot time t in the experimental shot.

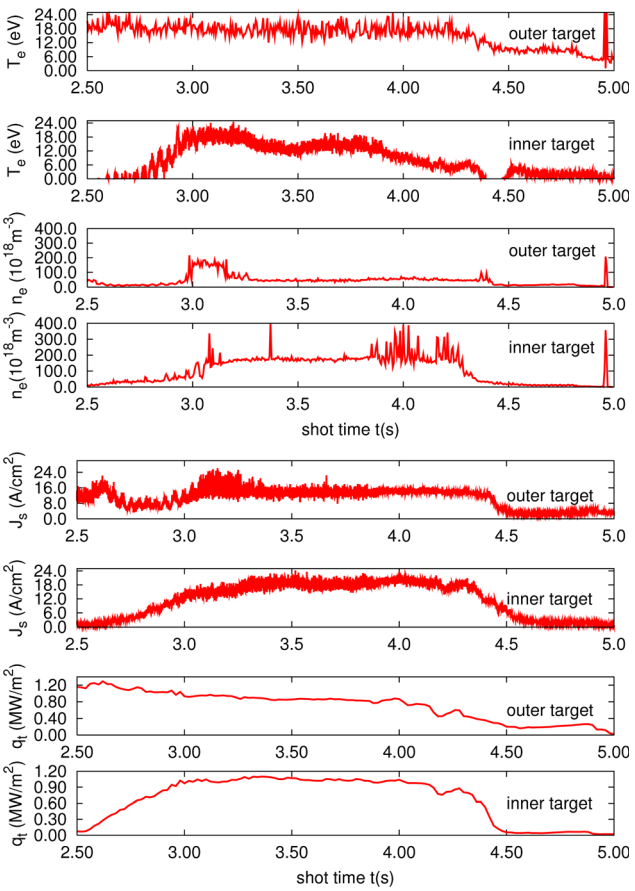

FIG. 2. The peak electron temperature T_e and density n_e, peak heat flux q_t, and ion saturation flux J_s to the target plates trace versus shot time t in the experimental shot.

T_e, density n_e, ion saturation current J_s, and power flux q_t have the apparent response to Ar seeding at the shot time $t = 4.4$ s, which also has about 0.4 s delay than the starting time of Ar seeding at the shot time $t = 4.0$ s: it means 0.4 s is needed for Ar to pass the seeding tube and arrive at the divertor plasma. After the shot time $t = 4.0$ s, T_e and q_t at the target plates begin to respond slowly to Ar seeding, so it is estimated that a small part of Ar may quickly pass the tube and arrives at divertor plasma earlier during Ar seeding. From Fig. 2, the peak electron temperature T_e, electron density n_e, ion saturation current J_s, and heat flux q_t to the divertor target plates decrease with the shot time t during the Ar puffing, illustrating the divertor plasma becomes partially detached. The full detachment of divertor plasma at the inner target plate can be estimated at the shot time $t = 5$ s because at that time $J_s \sim 0$ at the inner target plate.

The SOL/divertor plasma in the typical L-mode discharge is modelled. The modelling is carried out by using SOLPS5.2 which couples B2 to the neutral Monte-Carlo code Eirene. B2 solves the set of fluid transport equations that are similar to the set of Braginski equations. The numerical scheme based on these equations in SOLPS5.0 is quite satisfactory for the simulation of ohmic shots in tokamaks, but the convergence of the numerical scheme is much worse in some situations. In order to improve the numerical scheme a new equation system is used where strong radial particle and energy convective fluxes are replaced by poloidal fluxes

with the same divergence in SOLPS5.2. The new equation system is equivalent to the previous one and has better convergence when implemented into SOLPS5.2 code.[2]

In the modelling with SOLPS5.2, the multi-fluid species include the neutral deuterium, the deuterium ion D^+, electron e^-, and Ar impurity with neutral Ar, and all charged states from Ar^{+1} to Ar^{+18}. The neutral deuterium and neutral Ar are treated by Eirene; the ions are treated by B2. In the typical L-mode discharge on EAST tokamak, the plasma facing components (PFCs) consist of a plasma facing surface attached to an actively cooled heat sink. All plasma facing surfaces are made of multi-element doped graphite materials. So, the intrinsic impurity in the discharge is carbon. In the modelling the multi-fluid species do not include the intrinsic carbon impurity. The atomic processes, for example, ionization, recombination, and charge exchange are taken into account by using atomic physics data ADAS. Due to the uncertainties associated with the cross-field anomalous particle diffusion coefficient D, electron heat diffusivity χ_e and ion heat diffusivity χ_i, D, χ_e, and χ_i are adjusted and chosen in order to match the modelling results of the peak plasma temperature and heat fluxes at the target plates of divertor better to the experimental measurement by the assumption of $\chi_e = \chi_i$, which results in $D = 0.75\,\mathrm{m}^2/\mathrm{s}$ and $\chi_e = \chi_i = 1\,\mathrm{m}^2/\mathrm{s}$. D, χ_e, and χ_i are kept constant radially and at all times. The measured peak target values do not necessarily correspond to the peaks in the profiles because of insufficient spatial resolution of the measurements. Therefore, the uncertainties are too large for benchmarking the assumptions on D, χ_e, and χ_i against experimental data. The inward pinch velocity V_{in} is set to zero. The real MHD equilibrium in the shot is used for the production of the computational meshes in the modelling. The MHD equilibrium at the shot time $t = 4.25\,\mathrm{s}$, and the computational meshes produced by using the equilibrium are shown in Fig. 3. The drifts are not taken into account in the present modelling.

The boundary conditions at the boundaries of the computational region include the boundary conditions at the inner core boundary, the wall, the inner boundaries of private flux regions, and the divertor target plates. At the inner core boundary, the density of the deuterium ion D^+ is set as the density n_{ICB}. The neutral deuterium density n_0 at the inner core boundary is very low due to higher plasma temperature and stronger ionization, so the particle flux of neutral deuterium is set to zero. In order to show how high the density of Ar reaches at the inner core boundary due to Ar seeding, the particle fluxes of neutral Ar and all charged states of Ar are set to zero at the boundary. The density n_{ICB} and the heating power P are set as input parameters in the modelling. The total power flux from the inner core boundary to the computational region P_{in} can be deduced from the measured heating power P and the assumption about the radiation power in the core and SOL region. For electron and ion power fluxes to the computational region, P_e and P_i, no exact experimental data are available since a separation of P_e and P_i is not possible in the experimental measurement. Hence, for the present modelling an assumption that $T_e = T_i$ at the inner core boundary is made. The ratio P_i/P_e and T_e, T_i at the boundary are the code results with the boundary conditions

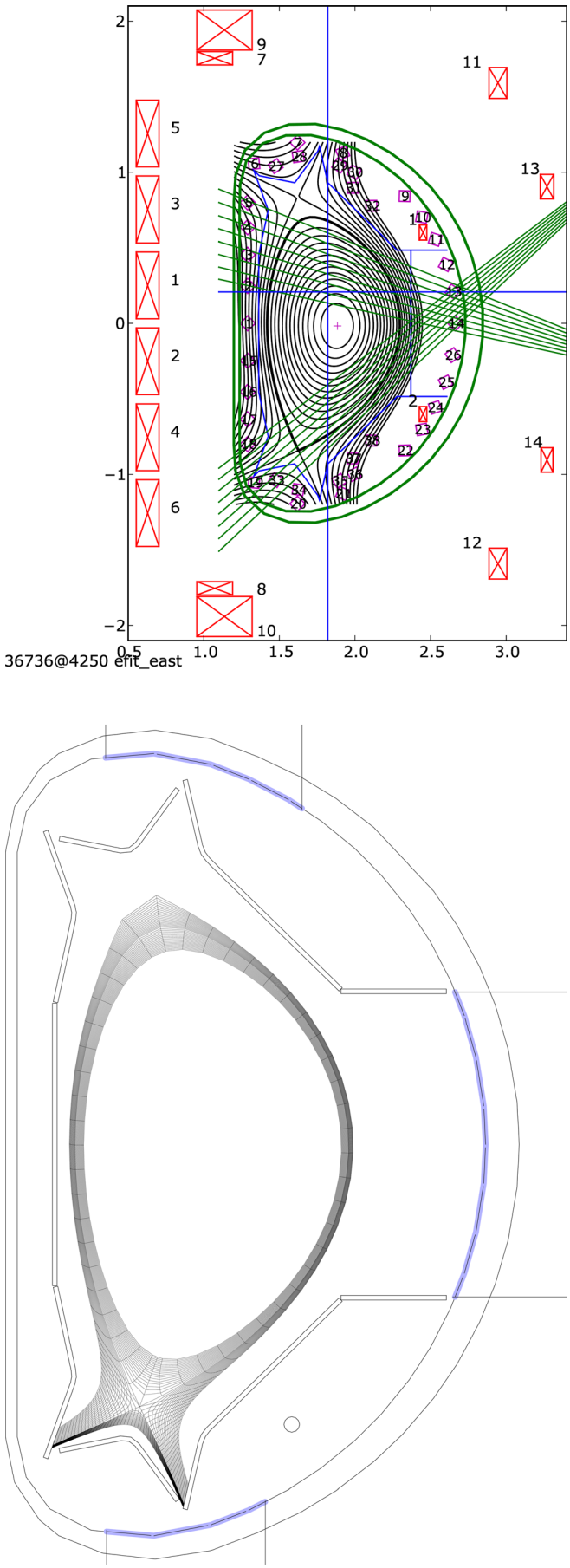

FIG. 3. The MHD equilibrium in the shot and computational meshes for the modelling.

$T_e = T_i$ and fixed input parameters of P and n_{ICB} or the separatrix density n_{esep}. For a given heating power P, it is assumed that 20% of the heating power is radiated as bremsstrahlung and cyclotron radiation from the core plasma according to the analysis of the power balance in the SOL plasma,[11] so $P_{in} = 80\%P$ is assumed for the present modelling. But, Ref. 11 discusses power balance in a high-power device with 100 MW heating power. The results of that analysis may not be applicable for the present modelling. So 20% radiated power in the core is assumed in the absence of radiation measurements or other relevant analysis. The normal current components are set to zero. The plasma density is maintained by the gas puffing near the inboard midplane. Because there is no measurement on rate of the gas puffing, the rate is adjusted so that the plasma density at the separatrix n_{esep} is about one third of the line-averaged plasma density $\bar{n}_e$, i.e., $n_{esep} \approx \frac{1}{3}\bar{n}_e$. The line-averaged plasma density $\bar{n}_e = 2.82 \times 10^{19}\,\mathrm{m}^{-3}$ is shown in the Table I, so n_{esep} is fixed in the modelling and n_{ICB} is the output of the code with fixed n_{esep}.

The SOL/divertor plasma is modelled before (at the shot time $t = 4$ s) and during (the shot time $t > 4$ s) Ar seeding in the typical discharge. The modelling results at $t = 4$ s without Ar seeding are used as initial conditions for the modelling with Ar seeding in the shot time $t > 4$ s. The code is run in time dependent mode and the time t corresponds to real time. Since time dependent process is simulated during the Ar seeding, it has to be sure that the characteristic time of code convergence is smaller than the typical time of the process, so the simulated situation is the quasistationary. Fig. 4 shows experimental and computational trace of the peak electron temperature T_e and the peak heat fluxes q_t at the inner and outer target plates versus the shot time t when Ar is seeding.

From Fig. 4 the modelling results show that before Ar seeding the peak electron temperature at the inner and outer targets is, respectively, $T_e = 11.65$ eV and $T_e = 14.70$ eV; the peak heat fluxes to the inner and outer targets are, respectively, $q_t = 1.11\,\mathrm{MW/m^2}$ and $q_t = 1.24\,\mathrm{MW/m^2}$. The peak electron temperature at the inner and outer targets is

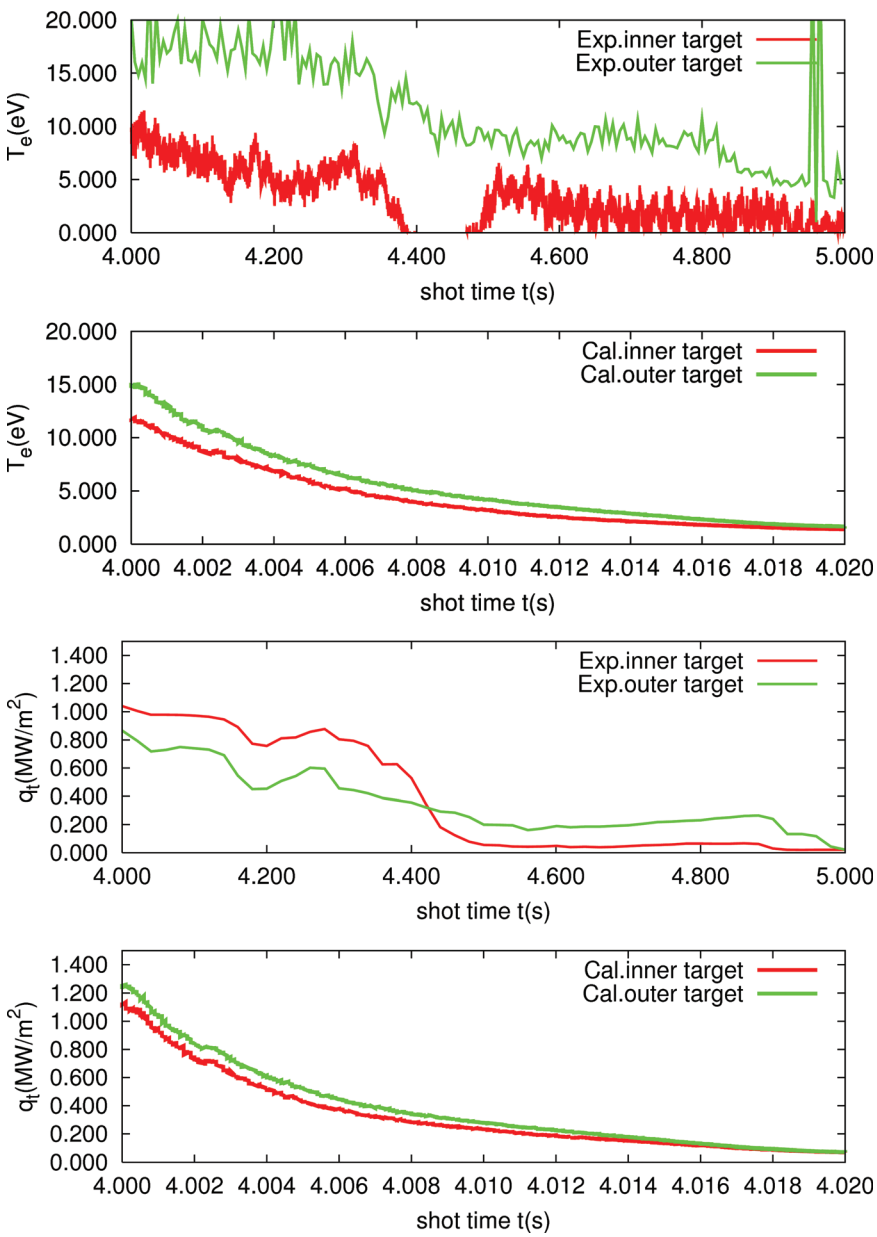

FIG. 4. The comparison between modelled and experimental results on the trace of peak electron temperature T_e and peak heat flux q_t to the target plates versus shot time t.

$T_e > 10.0\,\text{eV}$. With Ar seeding after $t = 4.0\,\text{s}$, the peak electron temperature and heat fluxes to the target plates begin to decrease with the increase of the shot time t. At the shot time $t = 4.01\,\text{s}$, i.e., the duration of Ar seeding $\delta t = 10\,\text{ms}$, the peak electron temperature and heat flux are, respectively, $T_e = 3.19\,\text{eV}$ and $q_t = 0.23\,\text{MW/m}^2$ at the inner target plate, $T_e = 4.20\,\text{eV}$ and $q_t = 0.28\,\text{MW/m}^2$ at the outer target plate. The maximum Ar density at the inner core boundary $n_{Ar-core} = 4.98 \times 10^{17}\,\text{m}^{-3}$, $n_{Ar-core}/\bar{n}_e = 1.77\%$. The peak electron temperature at the inner and outer targets $2.0\,\text{eV} < T_e < 5.0\,\text{eV}$. At the shot time $t = 4.02\,\text{s}$, i.e., the duration of Ar seeding $\delta t = 20\,\text{ms}$, the peak electron temperature and heat fluxes are, respectively, $T_e = 1.41\,\text{eV}$ and $q_t = 0.07\,\text{MW/m}^2$ at the inner target plate, $T_e = 1.67\,\text{eV}$ and $q_t = 0.073\,\text{MW/m}^2$ at the outer target plate, the maximum Ar density at the inner core boundary $n_{Ar-core} = 1.01 \times 10^{18}\,\text{m}^{-3}$, $n_{Ar-core}/\bar{n}_e = 3.58\%$. The peak electron temperature at the inner and outer targets $T_e < 2.0\,\text{eV}$. The modelling results show the cooling processes of divertor plasmas due to Ar seeding.

From Fig. 4 the modelling results on the trace of the peak electron temperature T_e and the peak heat fluxes q_t at the inner and outer target plates versus the shot time t when Ar is seeding are similar to the experimental measurement, but there is a major difference in time scales when Ar affects

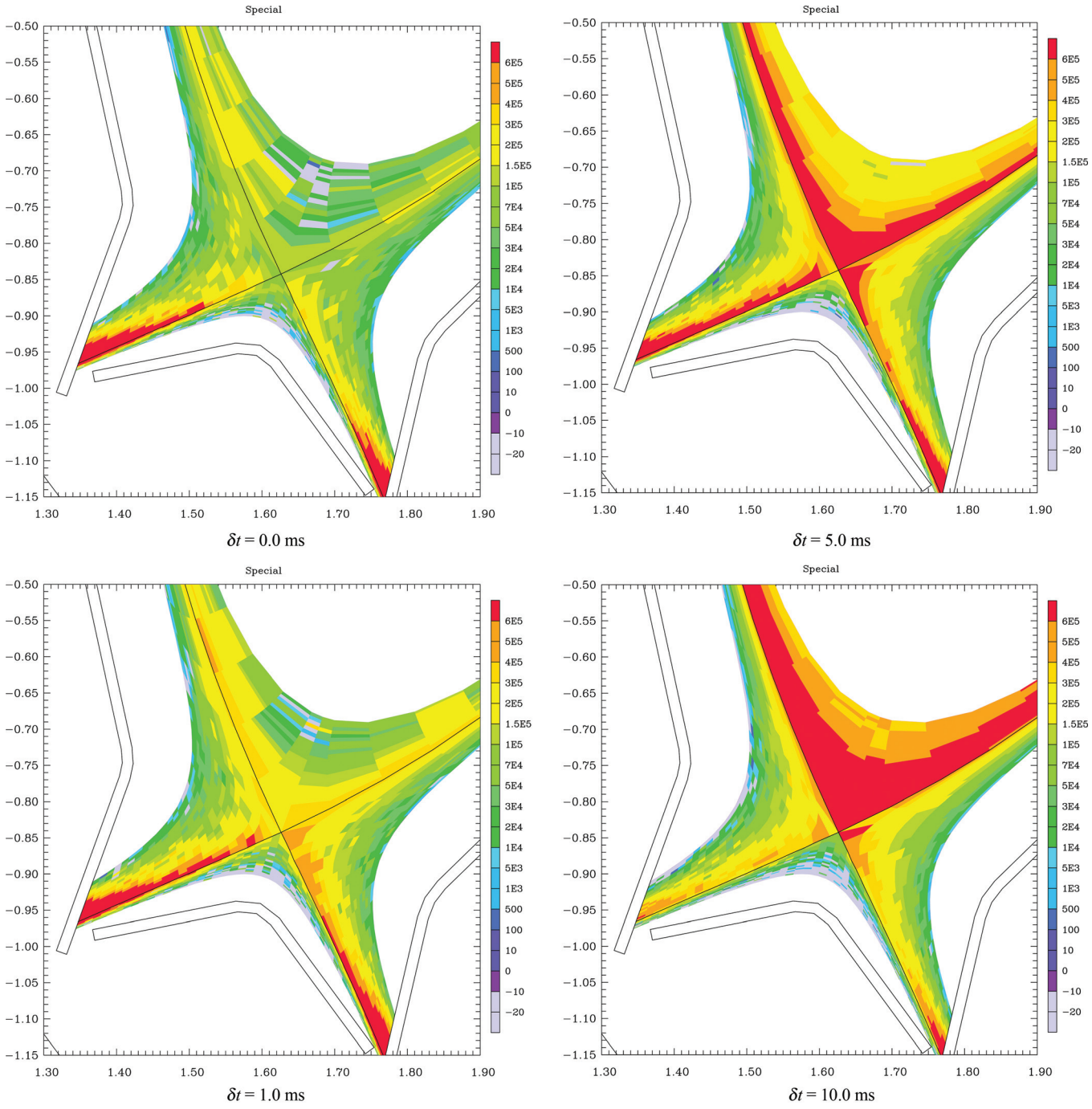

FIG. 5. The calculated volumetric radiation loss including electron cooling energy loss, the particle (ion or neutral) energy loss from the line radiation, bremsstrahlung radiation, the ionization and recombination in the computational region when Ar is seeding. The unit of energy loss is Wm^{-3}.

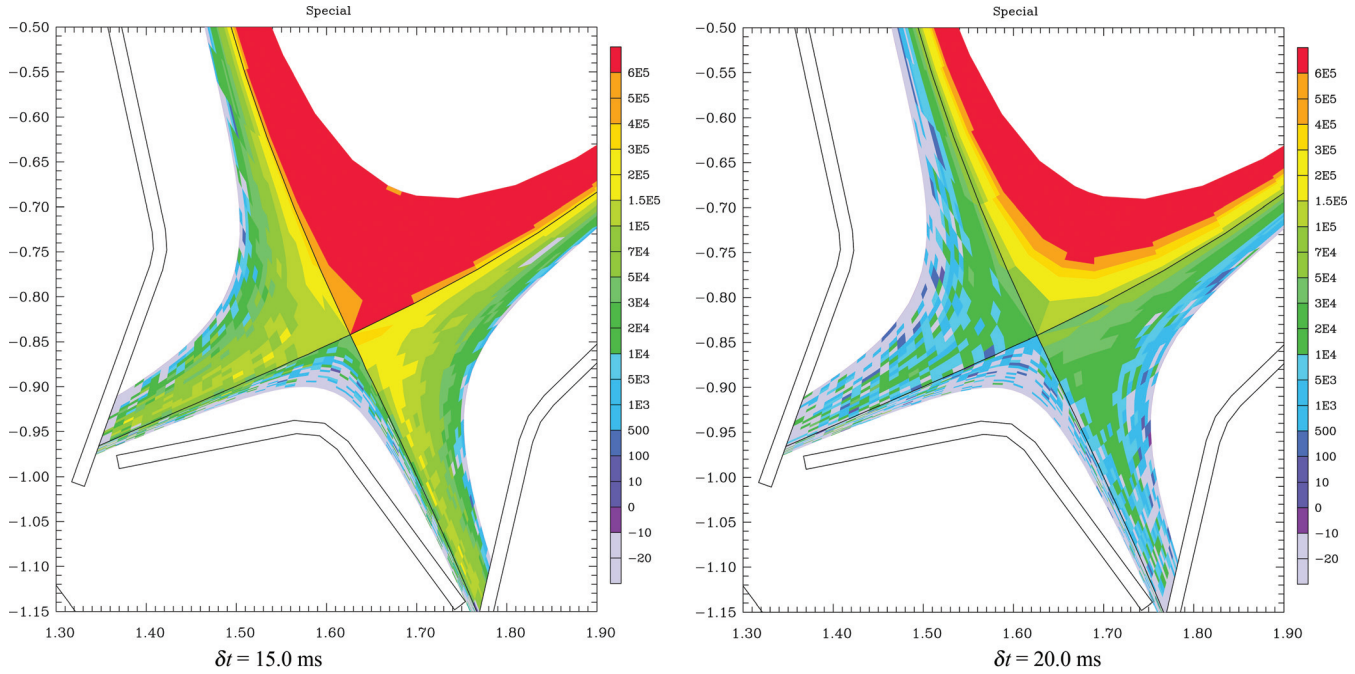

FIG. 5. (*Continued*.)

the plasma in between experiment and modelling. The peak electron temperature T_e and power flux q_t from the experiment response to Ar seeding later than that from the modelling, which may be caused by the fact that there are different Ar puff locations between the experiment and the modelling. In the modelling Ar is puffed near the separatrix strike point at the outer target plate, i.e., Ar is puffed from the boundary at the outer target of the computational domain. While in the experiment Ar starts off at the tube entrance which locates outside the torus, the Ar puff is situated in some distance from the puffing in the modelling. So, in the experiment it needs some time for Ar to pass the tube before it arrives at the separatrix strike point at the outer target plate and begins to effect the plasma. From Fig. 4 the time needed for Ar to pass the tube is about 0.4 s. It also appears from Fig. 4 that T_e and q_t decrease continuously in the experiment, starting from the time when Ar is injected at the shot time $t = 4$ s. The situation is different with the modelling results and may be explained by the reason that a small part of Ar may faster pass the tube and affects the plasma earlier, most of Ar affects the plasma at the shot time $t = 4.4$ s.

With the increase of shot time t and duration δt of Ar seeding, Ar is accumulated and the density of Ar in the plasma increases with the time, which causes the radiation front moves from the regions near the target plates of divertor towards the X-point and the core plasma. If Ar puffing rate is excessive, the excessive radiation from Ar can lead to plasma disruption. The experimental results in Figs. 1 and 2 show the discharge disrupts at about $t = 5.0$ s, which may be caused by excessive Ar puffing.

The volumetric radiation loss has been studied for the operation of radiative divertor with Ar seeding. Fig. 5 shows the modelling results of the volumetric loss including electron cooling energy loss, the particle (ion or neutral) energy loss from the line radiation, bremsstrahlung radiation, the ionization, and recombination in the computational region when Ar is seeding. In the operation without Ar seeding or at the beginning stage of Ar seeding (the duration of Ar seeding $\delta t = 0 - 1.0$ ms) the volumetric loss and the strong radiation region are in contact with or at a small distance from the divertor target. With the increase of the duration δt of Ar seeding, the volumetric radiation loss and the strong radiation region start to move towards the X-point, cooling the SOL plasma and lowering the plasma temperature in SOL. When $\delta t > 5.0$ ms the strong radiation region starts to move towards the core plasma, cooling the core plasma, which may produce effect on the properties of core plasma. The strong radiation region should be controlled within the divertor plasma by controlling the puffing rate of impurity in the radiative divertor. The study of the radiative divertor is at the beginning on EAST; at this moment it may be difficult to specify the puffing rate of impurity and control the strong radiation region in the experiment, so the predictive

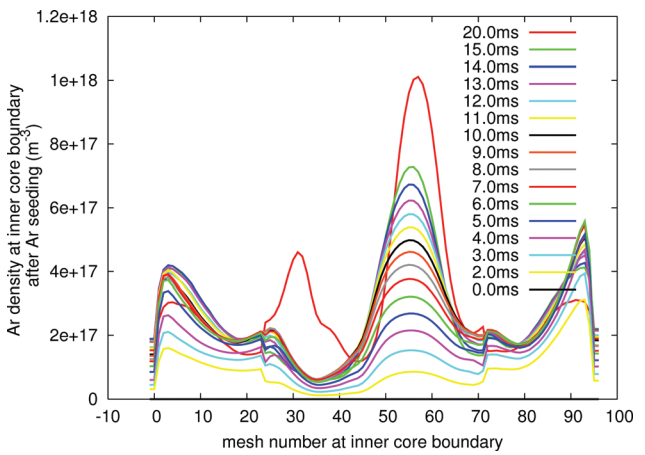

FIG. 6. The computational Ar density at inner core boundary for different duration δt(ms) of Ar seeding.

modelling is necessary for the study of the radiative divertor on EAST.

For different duration δt of Ar seeding, Fig. 6 shows maximum Ar density at inner core boundary $n_{Ar-core}$ during Ar seeding. At the shot time $t = 4.02$ s, i.e., $\delta t = 20$ ms, $n_{Ar-core} = 1.01 \times 10^{18}\,\mathrm{m}^{-3}$, $n_{Ar-core}/\bar{n}_e = 3.582\%$. With the increase of shot time t, $n_{Ar-core}$ increases, $n_{Ar-core}$ should be controlled in order to avoid effect of higher Ar density on core plasma.

III. CONCLUSIONS

The edge plasma code package SOLPS5.2 which couples the plasma fluid code B2 to the neutral Monte-Carlo code Eirene is used for the modelling of SOL/divertor plasma in the typical L-mode discharge with radiative divertor using Ar seeding on EAST tokamak. The real divertor geometry and the MHD equilibrium from the experimental shot are employed in the modelling. The heat flux $P = 80\% \times P_{in} = 1.18$ MW to the computational region and plasma density at the separatrix $n_{esep} = \frac{1}{3}\bar{n}_e$ are assumed for the modelling with the heating power $P_{in} = 1.475$ MW and the line-averaged electron density $\bar{n}_e = 2.82 \times 10^{19}\,\mathrm{m}^{-3}$ in the discharge. The modelling results show trace of the peak electron temperature T_e and the peak heat fluxes q_t at the inner and outer target plates versus the shot time t when Ar is puffing with rate $\Gamma = 1.26 \times 10^{20}\,\mathrm{s}^{-1}$.

The modelling results show that before Ar seeding the peak electron temperature at the inner and outer targets $T_e > 10.0$ eV. At the shot time $t = 4.01$ s, i.e., the duration of Ar seeding $\delta t = 10$ ms, the peak electron temperature at the inner and outer targets $2.0\,\mathrm{eV} < T_e < 5.0\,\mathrm{eV}$. The maximum Ar density at the inner core boundary $n_{Ar-core} = 4.98 \times 10^{17}\,\mathrm{m}^{-3}$, $n_{Ar-core}/\bar{n}_e = 1.77\%$. At the shot time $t = 4.02$ s, i.e., the duration of Ar seeding $\delta t = 20$ ms, the peak electron temperature at the inner and outer targets $T_e < 2.0$ eV. The maximum Ar density at the inner core boundary $n_{Ar-core} = 1.01 \times 10^{18}\,\mathrm{m}^{-3}$, $n_{Ar-core}/\bar{n}_e = 3.58\%$. The modelling results show the cooling processes of divertor plasmas due to Ar seeding and are similar to the experimental measurement, but there is a major difference in time scales when Ar affects the plasma in between experiment and modelling. It should be noted that in the future it will be necessary to monitor the some key data, for example, the peak plasma density and temperature, particle and heat fluxes at the targets, the profiles of plasma density and temperature, particle and heat fluxes at the target plates, and the time scales of the measured parameters, more carefully in the experiment in order to benchmark the core solutions better. The operation of the radiative divertor should be further optimized by experiments and modelling on EAST tokamak.

ACKNOWLEDGMENTS

This work was supported by the National Natural Science Foundation of China (No.10975158). The work also was supported partially by the JSPS-NRF-NSFC A3 Foresight Program in the field of Plasma Physics (NSFC No.11261140328) and the National Magnetic Confinement Fusion Science Program (Nos. 2010GB104005 and 2013GB109001). The authors would like to thank the EAST team for the experimental data.

[1]D. Wang, H. Guo, H. Wang, G. Luo, Z. Wu, J. Wu, W. Gao, L. Wang, Q. Li, and EAST Team, Phys. Plasma **18**, 032505 (2011).
[2]V. Rozhansky, E. Kaveeva, P. Molchanov, I. Veselova, S. Voskoboynikov, D. Coster, G. Counsell, A. Kirk, S. Lisgo, ASDEX-Upgrade Team, and MAST Team, Nucl. Fusion **49**, 025007 (2009).
[3]R. Schneider, X. Bonnin, K. Borrass, D. P. Coster, H. Kastelewicz, D. Reiter, V. A. Rozhansky, and B. J. Braams, Contrib. Plasma Phys. **46**(1-2), 3–191 (2006).
[4]D. P. Coster, X. Bonnin, G. Corrigan, G. S. Kirnev, G. Matthews, J. Spence, and Contributors to the EFDA-JET Work Programme, J. Nucl. Mater. **337–339**, 366–370 (2005).
[5]B. J. Braams, Contrib. Plasma Phys. **36**, 276 (1996).
[6]D. Reiter, J. Nucl. Mater. **196–198**, 80 (1992).
[7]D. Reiter, C. May, D. Coster, and R. Schneider, J. Nucl. Mater. **220–222**, 987 (1995).
[8]D. E. Post, J. Nucl. Mater. **220–222**, 143 (1995).
[9]ITER Physics Expert Group on Divertor, ITER Physics Expert Group on Divertor Modelling and Database, and ITER Physics Basis Editors, Nucl. Fusion **39**, 2391 (1999).
[10]H.-S. Bosch, D. Coster, R. Dux, C. Fuchs, G. Haas, A. Herrmann, S. Hirsch, A. Kallenbach, J. Neuhauser, R. Schneider, J. Schweinzer, M. Weinlich, ASDEX Upgrade Team, and NBI Team, J. Nucl. Mater. **241–243**, 82–91 (1997).
[11]D. N. Hill, B. Braams, J. Haines, J. Milovich, T. Rognlien, D. P. Stotler, and M. Ulrickson, Fusion Technol. **21**, 1263–1264 (1992).